

# Coronary Magnetic Resonance Angiography

Matthias Stuber, PhD,<sup>1–3\*</sup> and Robert G. Weiss, MD<sup>1,3</sup>

Coronary magnetic resonance angiography (MRA) is a powerful noninvasive technique with high soft-tissue contrast for the visualization of the coronary anatomy without X-ray exposure. Due to the small dimensions and tortuous nature of the coronary arteries, a high spatial resolution and sufficient volumetric coverage have to be obtained. However, this necessitates scanning times that are typically much longer than one cardiac cycle. By collecting image data during multiple RR intervals, one can successfully acquire coronary MR angiograms. However, constant cardiac contraction and relaxation, as well as respiratory motion, adversely affect image quality. Therefore, sophisticated motion-compensation strategies are needed. Furthermore, a high contrast between the coronary arteries and the surrounding tissue is mandatory. In the present article, challenges and solutions of coronary imaging are discussed, and results obtained in both healthy and diseased states are reviewed. This includes preliminary data obtained with state-of-the-art techniques such as steady-state free precession (SSFP), whole-heart imaging, intravascular contrast agents, coronary vessel wall imaging, and high-field imaging. Simultaneously, the utility of electron beam computed tomography (EBCT) and multidetector computed tomography (MDCT) for the visualization of the coronary arteries is discussed.

**Key Words:** coronary anatomy; angiography; motion compensation; contrast enhancement; pulse sequence design; heart

**J. Magn. Reson. Imaging 2007;26:219–234.**  
© 2007 Wiley-Liss, Inc.

THE CURRENT GOLD STANDARD for the diagnosis of coronary artery disease (CAD) is selective X-ray coronary angiography. Both in the United States and in Europe, approximately 1 million cardiac catheterizations are performed each year (1). However, X-ray coronary angiography is invasive and expensive, it exposes the patient and the technician to ionizing radiation, and

a small risk of some complications still exists. Thus, there is a strong need for more cost-effective, noninvasive, and patient-friendly techniques. Coronary magnetic resonance angiography (MRA) combines several advantages and great potential. MRA is a noninvasive, cost-effective imaging technique with a relatively high spatial resolution, high soft-tissue contrast, and the ability to generate any image plane in three dimensions. Additionally, there is no exposure to potentially harmful ionizing radiation with MRA. Therefore, the utility of coronary MRA has been investigated since the late 1980s (2,3). Although no coronary stenoses were identified in those early studies, it triggered further interest in this field. For successful coronary MRA data acquisition, a series of major obstacles must be overcome. The coronary arteries are relatively tortuous and small in diameter. Therefore, not only sufficient volumetric coverage but also a high spatial resolution is needed. For adequate visualization of the coronary arteries, an enhanced contrast between the coronary lumen and the surrounding tissue is crucial. Furthermore, the heart is subject to substantial motion due to its natural periodic contraction, as well as to breathing. Since both of these motion components are far greater than the actual size of the coronary artery dimensions, coronary MRA data acquisition with high contrast and spatial resolution is technically very challenging. In the present review, technical challenges and solutions are addressed, and the current state of the art of coronary MRI is discussed in the context of other emerging modalities, such as electron beam computed tomography (EBCT) and multidetector computed tomography (MDCT).

## TECHNICAL CONSIDERATIONS

### Suppression of Motion Artifacts

#### Suppression of Myocardial Motion Artifacts

*k*-Space segmentation, EKG triggering, and diastolic image acquisition. Volumetric high-resolution MRI data collection cannot be performed in real time. Therefore, data acquisition is commonly performed using R-wave triggering and data segments are obtained from up to 300 subsequent cardiac cycles (4), as shown in Fig. 1. It is assumed that cardiac motion is regular and highly repetitive. The collection of data over multiple cardiac cycles is called *k*-space segmentation. To minimize adverse effects of intrinsic myocardial motion, the segmented data are typically acquired in a short time win-

<sup>1</sup>Department of Radiology, Division of Magnetic Resonance Research, Johns Hopkins University, Baltimore, Maryland, USA.

<sup>2</sup>Department of Electrical and Computer Engineering, Johns Hopkins University, Baltimore, Maryland, USA.

<sup>3</sup>Department of Medicine, Cardiology Division, Johns Hopkins University, Baltimore, Maryland, USA.

\*Address reprint requests to: M.S., Johns Hopkins University Medical School, Russell H. Morgan Department of Radiology and Radiological Science; JHOC 4223, 601 North Caroline St., Baltimore, MD, 21287. E-mail: mstuber@mri.jhu.edu

Received October 18, 2005; Accepted February 2, 2007.

DOI 10.1002/jmri.20949

Published online in Wiley InterScience (www.interscience.wiley.com).

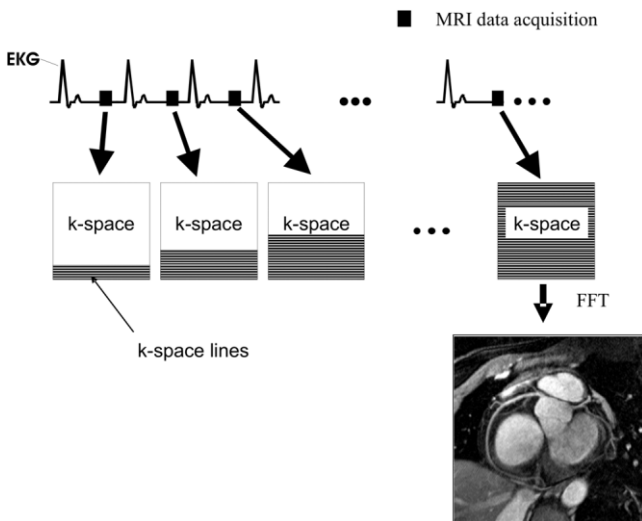


**Figure 1.** Suppression of intrinsic myocardial motion is obtained by (a) ECG triggering, (b) image data collection in late diastole during a period of minimal myocardial motion, and (c) image data collection in a narrow time window of <100 msec. Segments of  $k$ -space are filled in subsequent cardiac cycles (=  $k$ -space segmentation). FFT= fast Fourier transform.

dow (<100 msec) and during a period of minimal myocardial motion. Therefore, the period of minimal myocardial motion is typically visually inspected on a cine scan that precedes coronary MRA (5). Alternatively, the use of automated algorithms to detect the period of minimal myocardial motion has been suggested (6,7). Typically, a period of minimal myocardial motion is found in late diastole (8). In pediatric patients or patients with high heart rates, end-systolic imaging may be beneficial (9).

#### Suppression of Respiratory Motion Artifacts

**Breath-hold coronary MRA.** To compensate for respiratory motion, breath-holding was implemented early on. Two-dimensional (2D) breath-hold coronary MRA

relied on the acquisition of contiguous images, with the goal of surveying the proximal segments of the coronary arteries during serial breath-holds. More recently, three-dimensional (3D) breath-hold techniques for coronary MRA have also been implemented (10–15). Breath-hold approaches offer the advantage of rapid imaging and are technically easy to implement in compliant subjects. For coronary MRA techniques that utilize the first-pass contrast enhancement of intravenously injected extracellular contrast agents, breath-holding is now a requirement because it offers shorter acquisition times than non-breath-hold techniques. However, breath-holding strategies have several limitations. Some patients may have difficulty sustaining adequate breath-holds. In addition, it has been shown that during a sustained breath-hold cranial diaphragmatic drift (16) can occur, and is substantial in many cases (~1 cm). Among serial breath-holds, the diaphragmatic and cardiac positions frequently vary by up to 1 cm, resulting in registration errors (10,17). Misregistration results in apparent gaps between the segments of the visualized coronary arteries, which could be misinterpreted as signal voids from coronary stenoses. Finally, the use of signal enhancement techniques, such as signal averaging or foldover suppression, is significantly restricted by the duration of the applicable breath-hold duration. With breath-holding techniques, the spatial resolution of the images is also governed by the patient's ability to hold his/her breath. Thus, while breath-holding strategies are often successful with motivated volunteers, their applicability to the broad range of patients with cardiovascular disease is more limited.

**Free-breathing coronary MRA.** The development of respiratory navigators (18) for the suppression of respiratory motion artifacts enabled free-breathing coronary MRA data collection (19,20) (Fig. 2). Further advances included prospective adaptive real-time navigator technology (21), which enabled the acquisition of 3D coronary MRA during patient free-breathing and with sub-millimeter spatial resolution (22). While retrospective

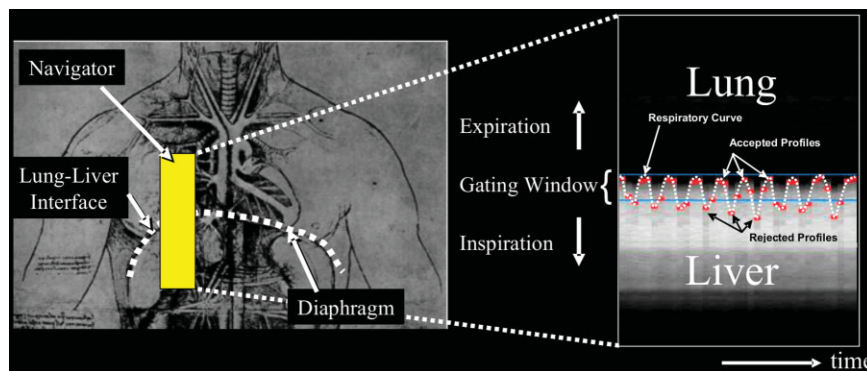


**Figure 2.** Navigator gating. The navigator signal is typically obtained from a moving structure, such as the lung–liver interface. For navigator signal generation, intersecting planes or 2D selective excitations can be used. A computer algorithm then detects the position of that interface (lung–liver interface) in real time. If such a computer-identified lung–liver interface position is found inside the gating window (the window width typically can be adjusted by the user), the  $k$ -space segment that is collected immediately after the navigator is accepted for reconstruction (black rectangles). However, if the lung–liver interface position is found outside the gating window (white rectangles), that  $k$ -space segment has to be remeasured in a later cardiac cycle. Adding navigator gating to an imaging sequence increases scanning time by a factor of ~2.

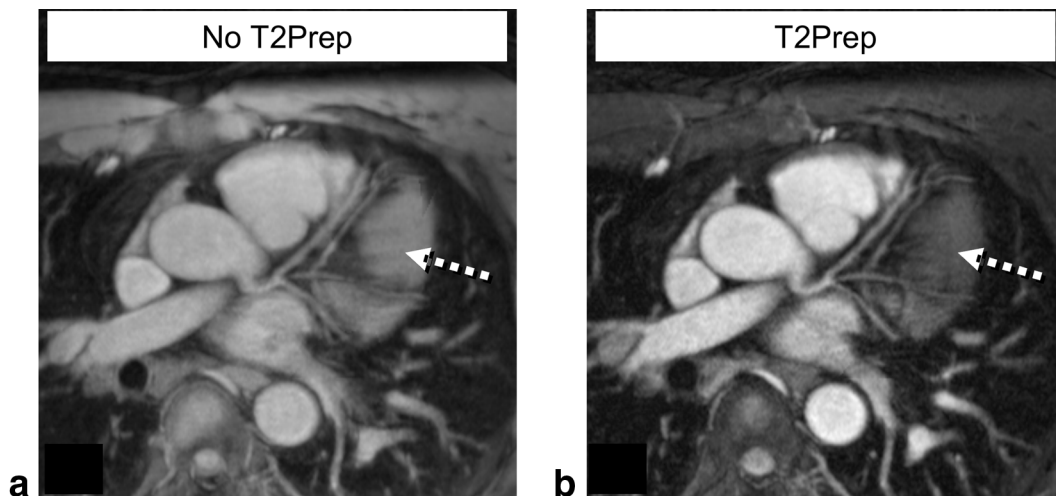


**Figure 3.** Coronary MRA of the left coronary system obtained in a healthy adult subject without (a) and with (b) T2Preparation (= T2Prep). The T2Prep enables endogenous contrast generation between tissue components with different T2's ( $T_{2\text{Blood}} = 250$  msec,  $T_{2\text{Myocardium}} = 50$  msec). With the T2Prep that typically precedes both image data collection and the navigator for free-breathing approaches, an enhanced contrast between the blood pool and the myocardium can be obtained (dashed arrow).

navigators have successfully been applied (19), prospective adaptive real-time volume position correction is not possible, and scanning times are typically prolonged compared to more advanced real-time navigator methods.

With the advent of parallel imaging and steady-state free precession (SSFP), 3D data collection during a single breath-hold became feasible (23). In a recent study by Jahnke et al (24), a direct comparison between 3D coronary MRA acquired with real-time navigator technology and that obtained in a single breath-hold was performed in 40 consecutive patients with suspected CAD. In that study it was concluded that navigator-gated and -corrected coronary MRA was superior in terms of image quality and diagnostic accuracy for stenosis detection.

### Contrast Enhancement

#### Endogenous Contrast Enhancement

In MRI the contrast between the coronary blood pool and the surrounding tissue can be manipulated by using the inflow effect (25) or applying MR prepulses (4,25–27). Non-exogenous contrast enhancement between the coronary arteries and the surrounding tissue has been obtained by the use of fat-saturation prepulses (25), magnetization transfer contrast (MTC) prepulses (28), and, more recently, T2 preparatory pulses (T2Prep) (26,29) that take advantage of natural T2 differences between blood and surrounding myocardium (Fig. 3). At 1.5T, the myocardium has a much shorter T2 (50 msec) than arterial blood (250 msec). With T2Prep, the longitudinal magnetization of both the coronary blood pool and the myocardium is tipped into the transverse plane, where both magnetization components experience a T2 decay. Since the T2 of the myocardium is shorter than that of arterial blood, a reduced longitudinal magnetization from the myocardium is obtained after a final 90° tip-up pulse. If imaging is performed at this point in time, more signal is obtained from the

arterial blood pool than from the myocardium, leading to an enhanced contrast. With these techniques, the coronary lumen appears bright, and the surrounding tissue, including fat and myocardium, appears with reduced signal intensity. An alternative to the bright-blood visualization of the coronary arteries is black-blood coronary MRA, in which the coronary lumen appears signal-attenuated while the surrounding tissue displays high signal intensity (30,31). Black-blood coronary MRA is typically obtained using a dual-inversion prepulse (25) in combination with a fast spin-echo (FSE) imaging sequence (Fig. 4).

#### Exogenous Contrast Enhancement

Contrast agents that are administered intravenously lead to a substantial reduction of blood T1. To take advantage of this shortened T1 in coronary MRA, an inversion prepulse typically precedes the imaging part of the sequence (27,32). With this mechanism, the signal of the myocardium is strongly attenuated. Imaging is performed at the zero crossing of the 1z-magnetization of the myocardium. At this point in time, the magnetization of the blood pool has almost fully relaxed because of the presence of the T1-shortening contrast agent. For these reasons, high contrast between the coronary blood pool and the surrounding tissue is obtained (Fig. 5). When extracellular contrast agents that quickly extravasate into the extracellular space are used, data collection during the first-pass is required, and therefore breath-holding is mandatory for the suppression of respiratory motion artifacts (13). However, a prolonged time window for contrast-enhanced coronary MRA data collection can be obtained with intravascular contrast agents (27,32–34). These agents typically remain in the vascular space for more than one hour, thus enabling the use of real-time navigator technology and 3D data collection with high spatial resolution.

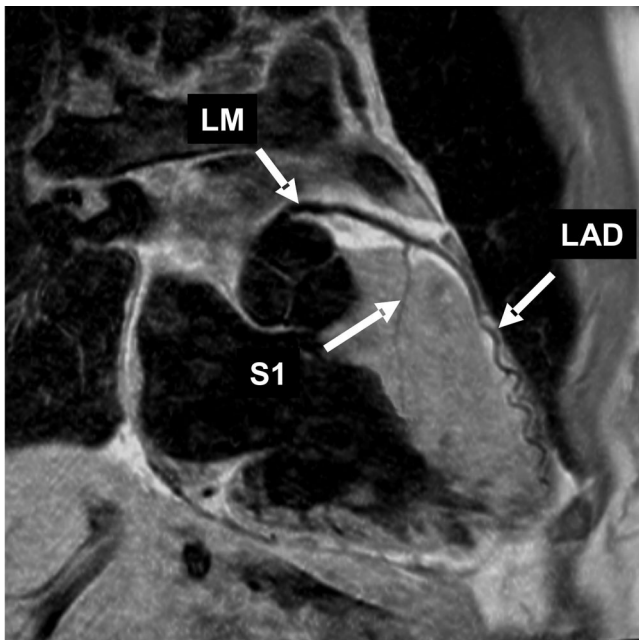


**Figure 4.** Black-blood coronary MRA of the left coronary system obtained in a healthy adult subject. S1 = septal branch. A contiguous 10-cm segment of the combined LM and LAD is shown. Black-blood contrast generation was obtained with a dual-inversion prepulse. Dual inversion is used for signal-nulling of the inflowing blood into the anatomy of interest. LM = left main; LAD = left anterior descending; S1 = septal branch. (Reprinted with permission from Ref. 31).

### Imaging Sequences

Because of the need for *k*-space segmentation and data collection in short acquisition intervals, conventional angiographic sequences that depend on continuous inflow of blood cannot easily be used. However, in the late 1980s, coronary MRA was obtained using spin-echo methods. With this technique the coronary lumen blood

pool is displayed signal-attenuated while the surrounding tissue, including epicardial fat and myocardium, appear signal-enhanced. However, with the availability of faster segmented *k*-space gradient-echo imaging in conjunction with fat saturation, a positive contrast between the coronary lumen blood pool and myocardium was obtained and the imaging duration per 2D slice was reduced to a single breath-hold. In 1991, substantial progress was also reported in a study that used spiral coronary MRA (35). In that study an improved spatial resolution and vessel conspicuity were demonstrated together with short scanning times, and higher-order branching vessels became visible for the first time. Despite this early success, spiral imaging currently is not widely used, even though a more recent study in which 3D spiral coronary MRA and 3D Cartesian segmented *k*-space gradient-echo imaging were compared concluded that the spiral technique is superior in signal-to-noise ratio (SNR), contrast-to-noise ratio (CNR), and vessel conspicuity (36). An example reformat of a coronary MRA obtained in a patient with x-ray-defined left anterior descending artery (LAD) disease is displayed in Fig. 6.

While most of the research and clinically oriented studies were performed using segmented *k*-space gradient-echo imaging, the utility of black-blood coronary MRA using dual-inversion and FSE imaging was revisited in 2001, and a direct comparison between black blood and bright blood was performed in a small patient study (37). No clear advantage of either method was reported; however, negative contrast is often difficult to interpret since the absence of tissue, calcifications, or motion artifacts may also lead to signal attenuation (30). One general disadvantage of dual-inversion black-blood techniques is the signal-attenuated appearance of calcifications, which can be misinterpreted as widely patent lumen (38). A big step forward in image quality was obtained using SSFP imaging (23,39). Example reformatted SSFP images obtained in a healthy adult

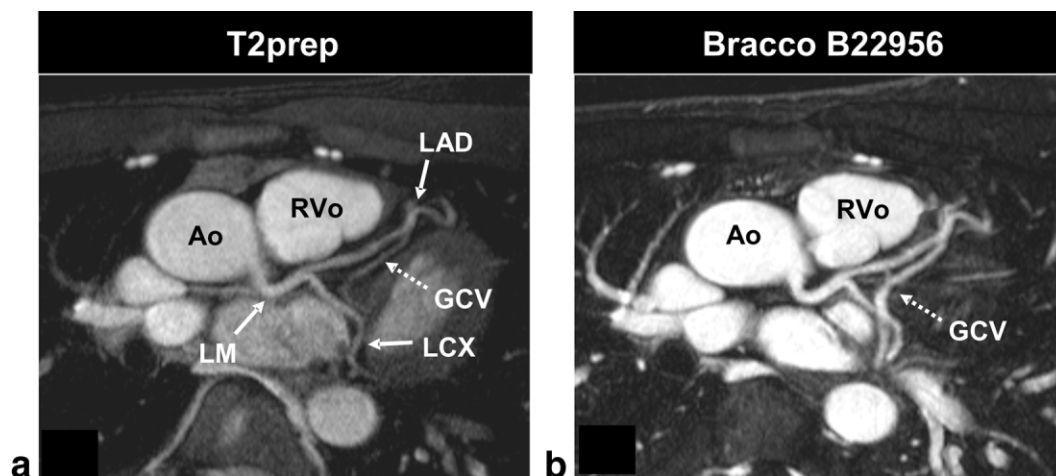


**Figure 5.** Coronary MRA obtained in the same healthy adult subject with endogenous (a, T2Prep) and exogenous (b, blood-pool agent) contrast enhancement. LCX = left coronary circumflex, GCV = great cardiac vein, Ao = ascending aorta, RVo = right ventricular outflow tract. With the blood-pool agent, a significantly enhanced contrast can be obtained that improves vessel conspicuity. The venous blood (GCV) is also enhanced by blood-pool agents. Coronary MRA with blood-pool agents is typically obtained with an inversion-recovery prepulse for signal-nulling of the myocardium. (Reprinted with permission from Ref. 32).

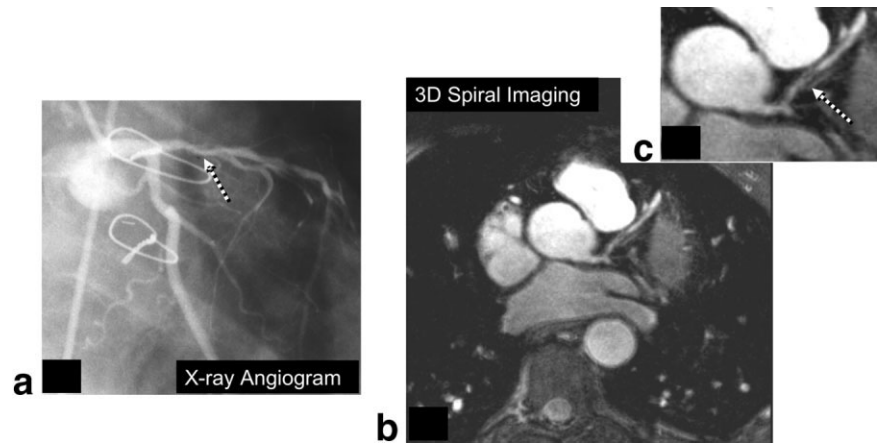


**Figure 6. a:** X-ray coronary angiogram obtained in a patient with CAD in the LAD. The location of the stenosis is confirmed on a coronary MRA obtained using an interleaved 3D spiral imaging sequence (**b** and **c**) during free breathing with navigator technology.

subject are displayed in Fig. 7. In combination with fat saturation and T2Prep, this leads to images with a very high contrast and vessel sharpness (40) (Fig. 7). In combination with navigators, the Cartesian SSFP technique is well suited for whole-heart imaging (41). The use of a radial version of SSFP imaging was reported (42,43), and it was found that although radial imaging is less susceptible to motion artifacts, a relative loss in SNR has to be considered (42). With the development of a 3D variant (“Kooshball”) of this “stack of radials” approach, isotropic spatial resolution for 3D whole-heart scanning became available (44). At 3T, both SSFP and segmented *k*-space gradient-echo imaging have been investigated. While excellent image quality has been obtained using SSFP (45), segmented *k*-space gradient-echo imaging was found to be superior in a preliminary study (46). This was attributed to enhanced magnetic field susceptibility at 3T in conjunction with specific absorption rate (SAR)-related limitations that do not permit the use of minimal TR at 3T.

### Volume Targeting

The coronary arteries have a relatively complex geometry and are often tortuous. This necessitates sufficient volumetric coverage. However, increased volume size typically requires prolonged scanning times. With an accurate targeting of the imaged volume parallel to the main segments of the coronary arteries, extensive segments of the coronary arteries can be displayed with high in-plane spatial resolution while scanning time is minimized. Volume targeting for coronary MRA (11) can be obtained using the volume coronary angiography using targeted scans (VCATS) approach (12) or a three-point planscan tool (47). It is important to mention that volume targeting is performed on a scout scan that is acquired under conditions identical to the subsequent high-resolution acquisition. This means that scan volume localization for free-breathing, late-diastolic, 3D high-resolution coronary MRA must be performed on a low-resolution scout scan that is acquired both during free breathing and in late diastole

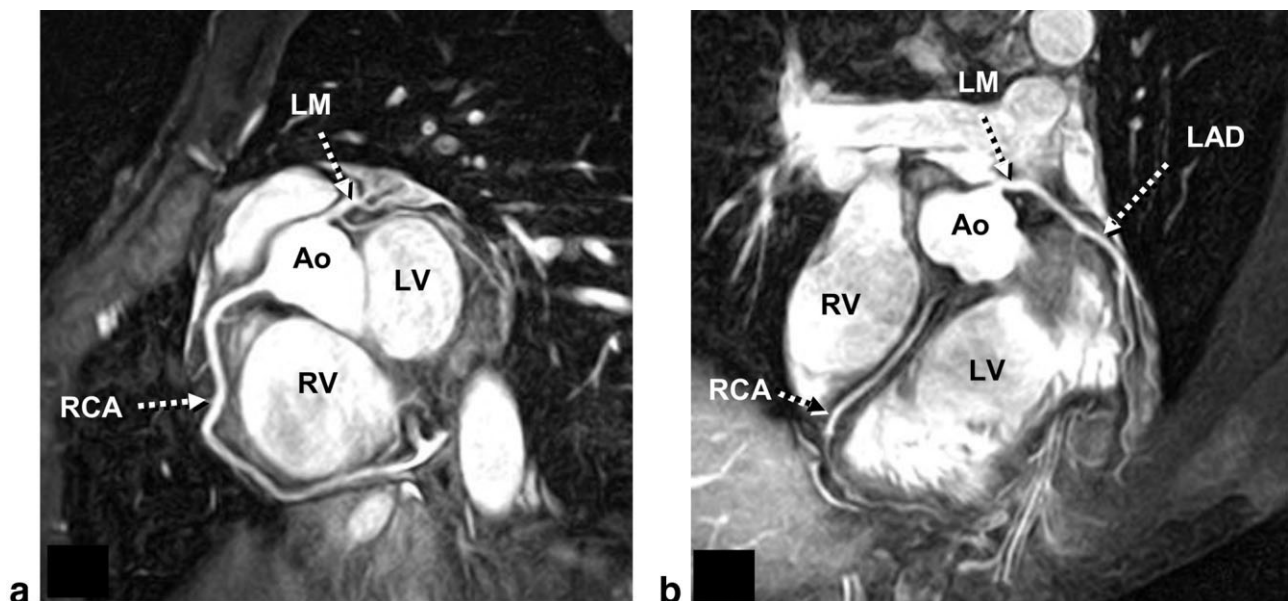


**Figure 7.** SSFP coronary MRA of the right (**a**) and left (**b**) coronary systems of two healthy adult subjects, acquired using free-breathing and navigators. The use of SSFP leads to high SNR, CNR, and vessel conspicuity. Ao = ascending aorta; RV = right ventricle; LV = left ventricle; LAD = left anterior descending; RCA = right coronary artery.

(47). Ideally, the duration of the acquisition intervals within the cardiac cycle of both the scout scan and the high-resolution scan should be identical. While volume-targeted approaches help to reduce scanning time and simultaneously take advantage of an enhanced inflow contrast, serial measurements are still needed to image the major coronary segments, which increases the overall scanning time. For these reasons, whole-heart 3D coronary MRA may be more advantageous.

### Whole-Heart Coronary MRA

Volume-targeted coronary MRA has been used successfully in many patient and volunteer studies, and is currently the only technique with multicenter experience (48). However, the need for accurate localization of the coronary arteries makes the technique operator-dependent, and only limited access to more distal and branching vessels has been obtained using this approach (48). For these reasons, a whole-heart coronary MRA approach was suggested by Weber et al (41) in 2003. This powerful technique minimizes operator interaction for the localization of the imaged volume, and it encompasses the whole heart, which enables access to more distal coronary segments than the targeted approach. The development of this technique was critically supported with the advent of parallel imaging and SSFP. Whole-heart coronary MRA is commonly performed during free breathing using real-time navigator technology and contrast enhancement is obtained using a T2Prep in conjunction with spectrally selective fat saturation (41,44). Inflow contrast is generally reduced in large-volume acquisitions, but in part this is compensated for by the high intrinsic contrast of SSFP imaging. A volume-rendered reconstruction of such a

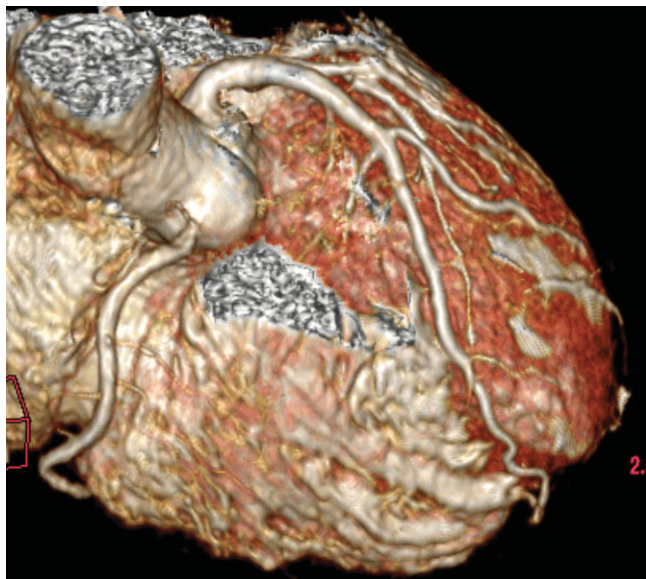


**Figure 8.** Volume-rendered whole-heart coronary MRA obtained using navigator-gated and corrected free-breathing 3D SSFP imaging with T2Prep and spectrally selective fat saturation. With a SENSE factor of 2, the total imaging duration was 10–15 minutes. (Image courtesy of Hajime Sakuma, Mie University, Japan.)

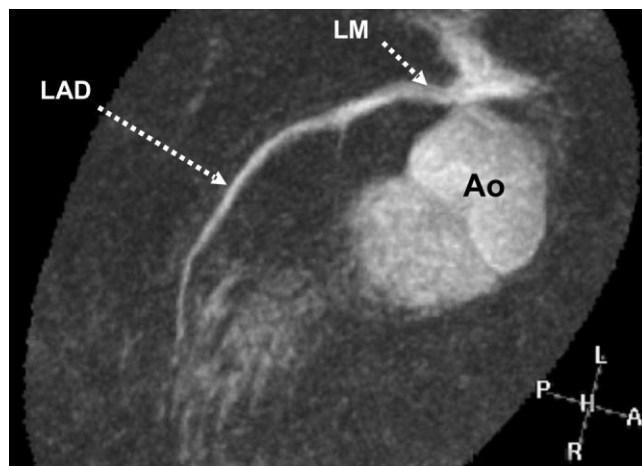


**Figure 9.** The LM and LAD obtained in a healthy adult subject using ASL. 2D selective cylindrical spin labeling in the Ao preceded 2D spiral imaging by 350 msec. During these 350 msec, aortic blood entered the LM and LAD, and a 10-cm contiguous segment can be visualized selectively and exclusively. LM = left main; Ao = ascending aorta; LAD = left anterior descending.

whole-heart coronary MRA is displayed in Fig. 8. This data set was acquired and reformatted as described in Ref. 49. Currently, whole-heart coronary MRA data acquisition is still relatively lengthy (10–15 minutes during free breathing) and the use of algorithms that compensate for respiratory drift (24–50,51) or respiration-induced myocardial deformation (52,53) will add further value to this elegant approach. In conjunction with larger cardiac-dedicated coil arrays, parallel imaging with undersampling in two rather than only one phase-encoding direction will contribute to further significant reductions in scanning time (54). However, this requires large coil arrays (55), and an optimized coil geometry for coronary MRA is currently the subject of ongoing research (56).

### VISUALIZATION OF THE CORONARY ANATOMY

On X-ray coronary angiograms, the coronary lumen blood pool displaced by iodinated contrast agent is exclusively displayed in a 2D projection. However, on coronary MRA, not only the coronary lumen blood pool but also the surrounding tissue (including epicardial fat, myocardium, and blood in the atria, ventricles, and great cardiac vessels) are simultaneously displayed (Figs. 3–8). On bright-blood coronary MRA, the coronary blood-pool appears signal-enhanced while epicardial fat and myocardium display signal attenuation. On black-blood coronary MRA, the blood pool is visualized signal-suppressed and the surrounding structures display with high signal intensity. Since the coronary anatomy cannot be displayed exclusively, semiautomatic 3D reformatting algorithms are sometimes used (57). These techniques permit a 3D visualization of the coronary arterial system. More recently, arterial spin labeling (ASL) techniques have also been introduced (58). With this technique, as shown in Fig. 9, the coronary lumen blood pool can be visualized exclusively, selec-

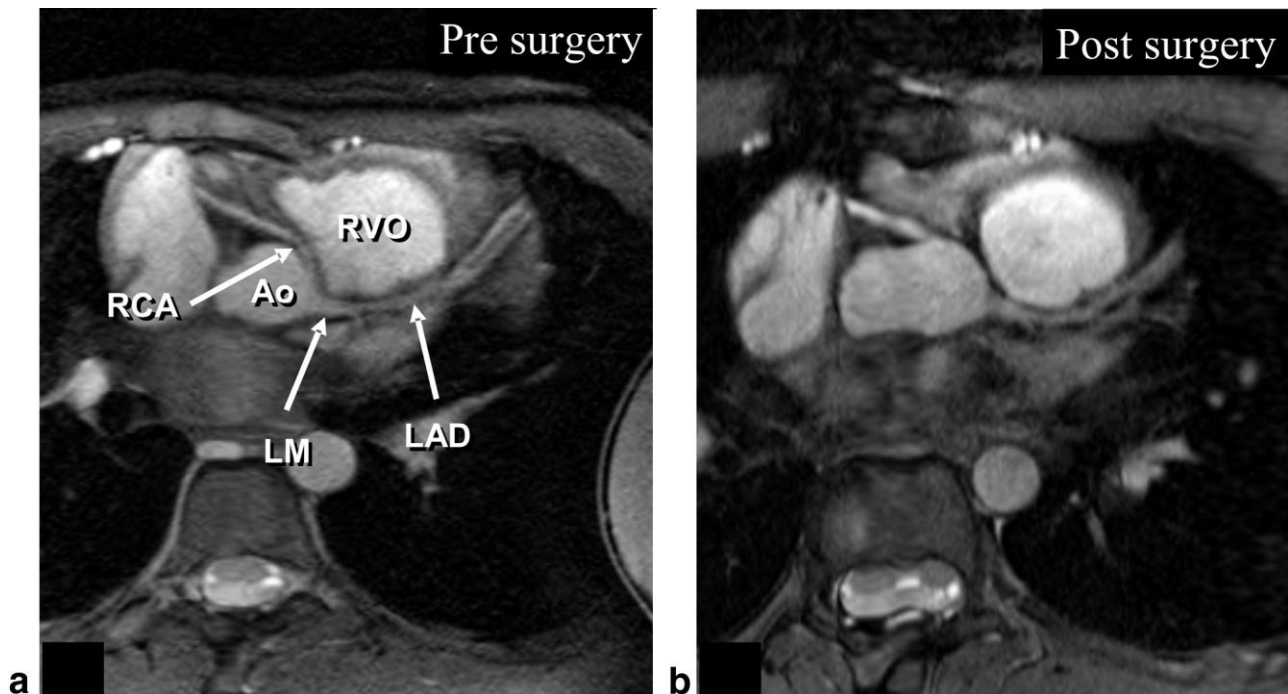


**Figure 10.** Coronary MRA obtained in a pediatric patient. On the left (a), the anomalous origin of the RCA (originating from the LM) that runs between the Ao and the RVO is observed. These data were obtained presurgery. Postsurgery, the RCA originates from the right coronary cusp (b), while an enhanced artifact level can be attributed to metallic implants (sternal wires) postsurgery. (Reprinted with permission from Ref. 63). RVO = right ventricular outflow tract; Ao = ascending aorta; LM = left main; LAD = left anterior descending; RCA = right coronary artery.

tively, and in 3D without user-assisted postprocessing or segmentation. However, since spin labeling necessitates the subtraction of a labeled and a nonlabeled data set, scanning time is doubled and experience is very limited at the present time.

#### **Visualization of the Normal Coronary Anatomy**

In general, the LAD and the right coronary artery (RCA) are relatively easier to image compared to the left circumflex artery (LCX) due to their closer proximity to the receiver coil. Consequently, the length of the LAD and RCA visualized in several studies is typically longer than that of the LCX, ranging from 24 to 116 mm for the LAD, 34 to 126 mm for the RCA, and 11 to 97 mm for the LCX (59). The LCX is more difficult to visualize because of its relative distance to the coil and its close proximity to the great cardiac vein. While contrast agents support the visualization of the LCX, venous enhancement has to be considered. In normal subjects the diameter of the coronary vessels as determined by coronary MRA is similar to X-ray angiographic and reference anatomic data (60,61).

#### **Visualization of Anomalous Coronary Arteries and Coronary Aneurysms in Kawasaki Disease**

Anomalous coronary arteries are a well known but rare cause of myocardial ischemia and sudden death in children and young adults. The projectional nature of conventional X-ray angiography often leads to difficulty in defining the course of anomalous vessels, especially in

regard to the great vessels. Studies have documented the high accuracy of coronary MRA for the noninvasive detection and definition of anomalous coronary arteries in patients with suspected anomalous coronary arteries or congenital conditions associated with anomalous coronary arteries (62,63). With increasing clinical experience, coronary MRA will likely emerge as the gold standard for the diagnosis of this condition. The ability of coronary MRA to identify the proximal coronary vessels reliably, coupled with the inherent 3D nature of MRI and the ability to generate tomographic images in any orientation, renders this technique uniquely suited for the noninvasive study of anomalous coronary arteries (62,63) (Fig. 10). Further, 3D coronary MRA has shown to be very effective for both visualizing and measuring the dimensions of coronary aneurysms in pediatric patients with Kawasaki disease (64) (Fig. 11).

#### **Visualization of CAD**

Although current breath-hold coronary MRA techniques have relatively limited in-plane spatial resolution, the technique has been shown to identify proximal coronary stenoses in several clinical series. Gradient-echo techniques depict focal stenoses as signal voids. In one of the earliest patient studies that prospectively compared X-ray coronary angiography and coronary MRA (65), a segmented *k*-space 2D breath-hold ECG-gated gradient-echo sequence was used. The overall sensitivity and specificity of the 2D coronary MRA technique for correctly classifying individual vessels as hav-

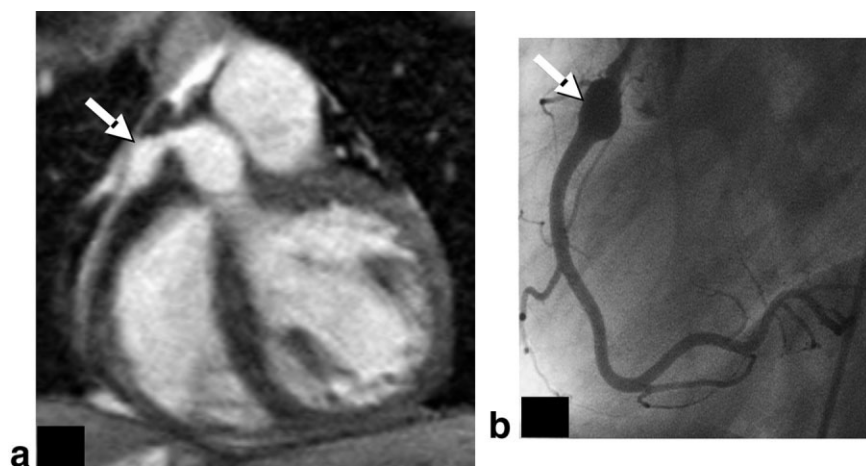


**Figure 11.** Coronary MRA (a) and corresponding X-ray angiogram (b) from a pediatric patient with Kawasaki disease. The location of the aneurysm can clearly be identified on the MRA and is confirmed on the X-ray angiogram. (Reprinted with permission from Ref. 63).

ing or not having significant CAD (50% diameter on conventional contrast angiography) were 90% and 92%, respectively. Subsequent studies (66–70) have reported variable sensitivity and specificity values for the detection of significant CAD. Explanations for this variability in these single-center studies include differences in the MR sequences used, inadequate patient cooperation with breath-holding, and irregular rhythms, all of which contribute to image degradation. Newer breath-hold (14) and non-breath-hold approaches for 3D coronary MRA have also demonstrated the ability of this technique to detect coronary stenoses. The first and currently only multicenter trial to prospectively compare coronary MRA and X-ray coronary angiography using common hardware, software, and methodology was reported in 2001 (48). Eight international centers enrolled subjects in this study. In comparison to the gold standard, X-ray coronary angiography, a sensitivity of 93% and specificity of 42% with a positive and negative predictive value of 70% and 81%, respectively, was obtained for the identification of significant CAD. For left main (LM) or three-vessel disease, a sensitivity of 100%, a specificity of 85%, a positive predictive value of 54% and a negative predictive value of 100% were reported. A major finding was that free-breathing, sub-millimeter 3D coronary MRA can accurately identify significant proximal and mid coronary disease, while nonsignificant coronary disease can be excluded with high confidence. The specificity (false-positive readings) still remains to be improved, and quantitative stenosis grading remains to be investigated. That study also concluded that access to more distal and smaller-diameter branching vessels is now needed. Therefore, the use of the whole-heart technique was investigated in a patient study by Sakuma et al (49) (Fig. 12). In that study, which included 20 patients, a sensitivity of 82% and a specificity of 91% were obtained for the identification of significant CAD when compared to the gold standard, X-ray coronary angiography. The average scanning time was  $13.8 \pm 3.8$  minutes during free breathing.

#### **Visualization of Coronary Bypass Grafts**

The value of MRI for assessing coronary bypass graft patency was investigated in early studies with ECG-

triggered spin-echo (71) and gradient-echo techniques (71,72). In those early studies, visualization of grafts and graft patency was limited by cardiac and respiratory motion artifacts. As a result, stenoses could not be identified or quantified. With the advancement of technology, data collection during one breath-hold became feasible (73). While all occluded grafts were successfully identified using breath-holding (73), only 67% of the patent grafts were correctly diagnosed. Limitations included diaphragmatic drift during a breath-hold, the need for serial breath-holds, and the dependence of the maximum spatial resolution on the patient's ability to hold his/her breath. More advanced alternatives for respiratory motion compensation included the use of retrospective respiratory navigators (19). This technique removed the constraints related to breath-holding and enabled 3D acquisition with an in-plane spatial resolution of  $\sim 1$  mm (74). With this method, the sensitivity and specificity for the assessment of graft patency were 87% and 100%, respectively, but luminal stenoses still could not be assessed reliably. More recently, Langerak et al (75) adopted navigator-gated and -corrected coronary MRA for the assessment of vein grafts (Fig. 13). With this method, a sensitivity of 83% and specificity of 98% for the definition of graft occlusion were obtained in 38 subjects. Furthermore, a fair diagnostic accuracy for assessing the severity of vein graft stenosis was reported for the first time. However, it should be noted that imaging of arterial grafts is often more difficult, primarily because of metallic implants.

#### **Coronary Flow Imaging**

MR flow mapping has been validated in animals by comparison with ultrasound (76–79), and in humans by comparison with Doppler guidewire measurements (80–84). An excellent correlation between MRI and Doppler guidewire measurements was found in humans for coronary flow and flow reserve measurements (80,83,85) in different patient subgroups.

#### **Coronary Vessel Wall Imaging**

Imaging of the coronary artery vessel wall using MRI is very challenging because of the small dimensions and the constant motion of the coronary arteries. Simulta-

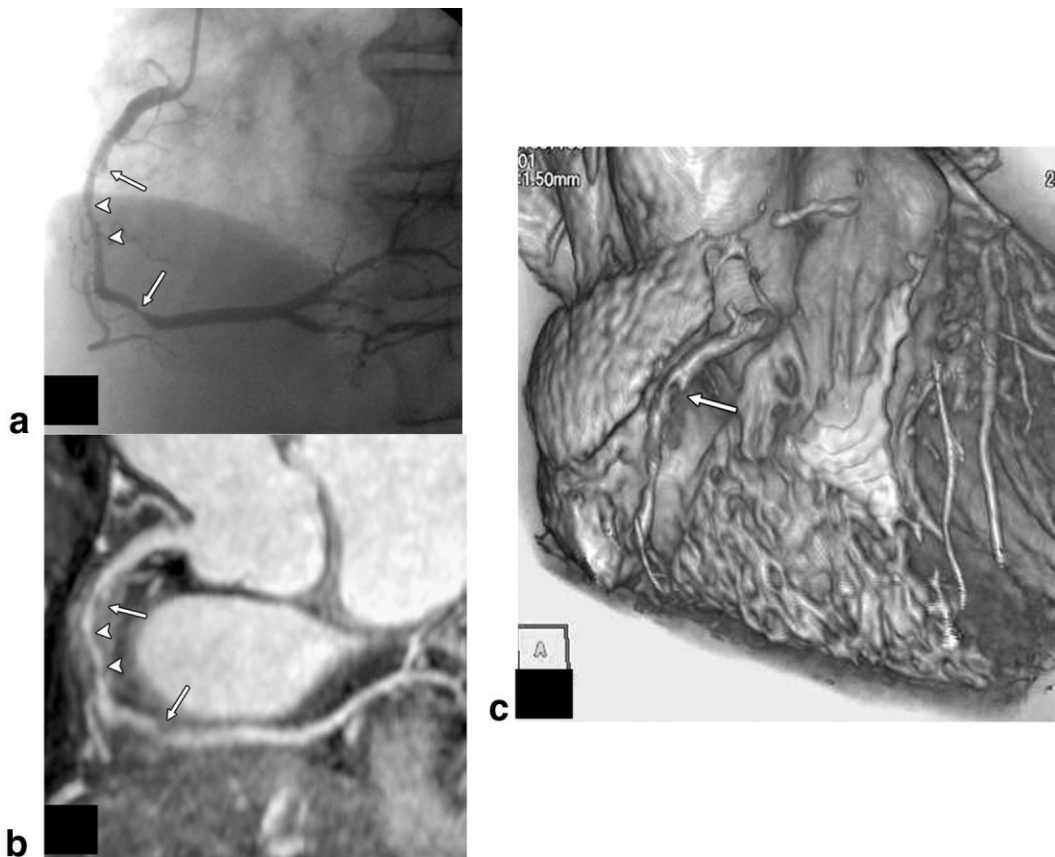


**Figure 12.** X-ray coronary angiogram (a), multiplanar reformat of a whole-heart coronary MRA data set (b), and volume-rendered visualization of the same data set obtained in a patient with RCA disease (arrows). (Reprinted with permission from Ref. 49).

neously, a high contrast between the coronary lumen blood pool and the surrounding coronary vessel wall is mandatory.

The first successful implementations of coronary vessel wall imaging in humans included the use of a dual-inversion FSE sequence. Using this method, single slices of the coronary artery vessel wall can be acquired during a prolonged breath-hold period, and relative thickening of the coronary arterial vessel wall was successfully demonstrated in selected cases (86). Subsequently, and to remove the limitations associated with breath-holding, this technique was extended with navigators for free-breathing data acquisition (87).

More recently, the free-breathing navigator approach was combined with 3D spiral imaging in conjunction with a “local inversion” technique (88). With this method, a high image quality can be obtained because of the high SNR associated with 3D imaging on the one hand and the signal-efficient spiral readout on the other hand. This enables a larger anatomical coverage, while the reconstructed slices are much thinner than those of the earlier 2D approaches. Therefore, it is now possible to visualize long, contiguous sections of the coronary artery vessel wall, as shown in Fig. 14. Additionally, the spiral approach permits data acquisition in a short acquisition window of 50 msec only. Therefore, the adverse effects of intrinsic myocardial motion can be suppressed more effectively and the technique may

be less susceptible to RR variability. The disadvantages of this technique include the prolonged scanning time of ~12 minutes during free breathing (image acquisition during every other RR interval).

In a study using this local-inversion 3D spiral technique (89), 12 adult subjects (six clinically healthy subjects and six patients with nonsignificant CAD (10–50% X-ray angiographic diameter reduction)) were examined with the use of a commercial 1.5T CMR scanner. Free-breathing 3D coronary vessel wall imaging was performed along the major axis of the RCA with isotropic spatial resolution ( $1.0 \times 1.0 \times 1.0 \text{ mm}^3$ ). The proximal vessel wall thickness and luminal diameter were objectively determined with an automated algorithm (29). The 3D vessel wall scans allowed for visualization of the contiguous proximal RCA in all subjects. The mean vessel wall thickness ( $1.7 \pm 0.3$  vs.  $1.0 \pm 0.2 \text{ mm}$ ) was significantly increased in the patients compared to the healthy subjects ( $P < 0.01$ ). However, the lumen diameter measurement ( $3.6 \pm 0.7$  vs.  $3.4 \pm 0.5 \text{ mm}$ ,  $P = 0.47$ ) was similar in both groups. Therefore, free-breathing 3D black-blood coronary MRI provides a non-invasive technique for identifying increased coronary vessel wall thickness while preserving lumen size in patients with nonsignificant CAD, consistent with a “Glagov-type” outward arterial remodeling (90). This novel approach has the potential to quantify subclinical disease (Fig. 14).

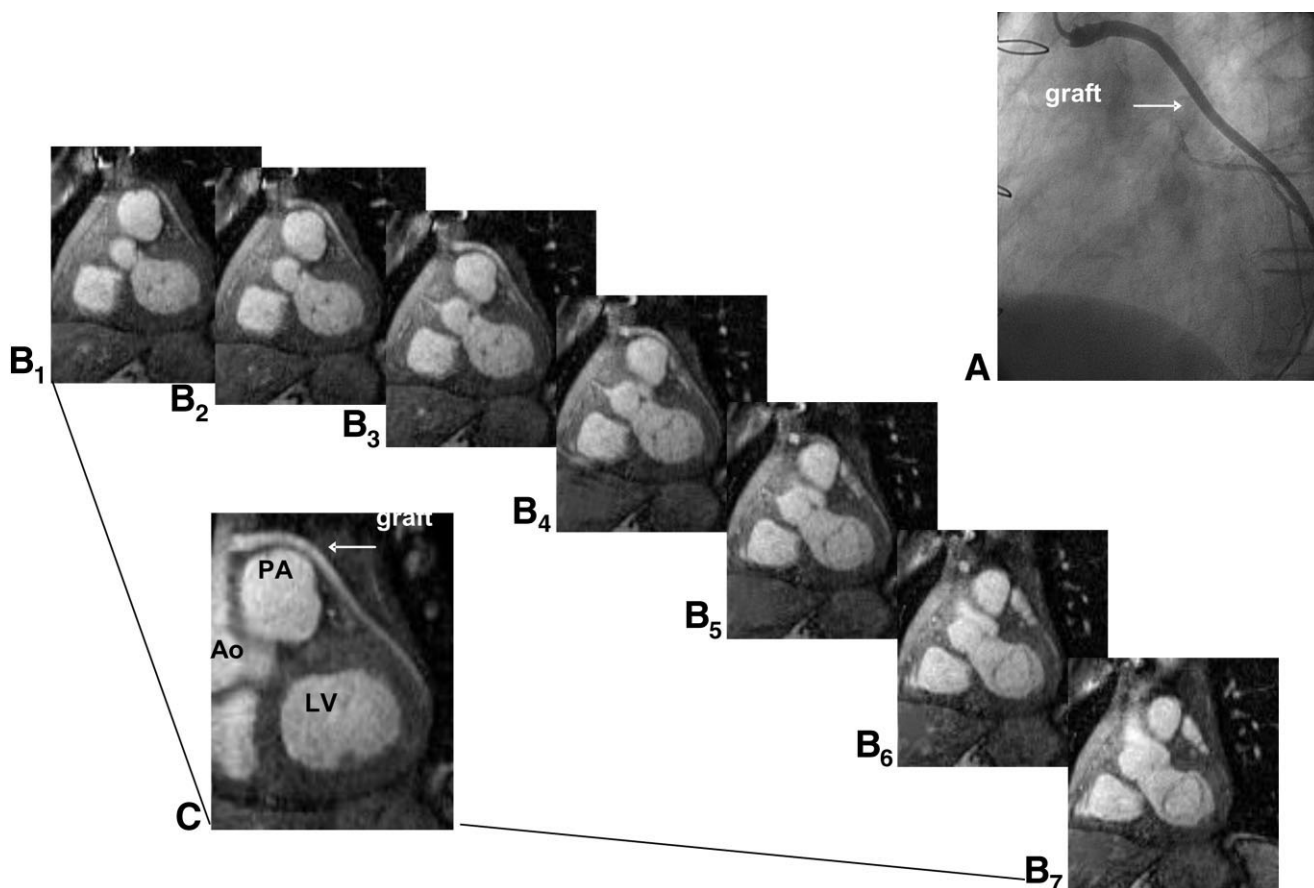


**Figure 13.** X-ray angiogram (a), adjacent slices of a 3D coronary MRA (b1–b7), and multiplanar reformatted visualization (c) of an X-ray angiographically patent coronary artery bypass graft. Ao = ascending aorta, LV = left ventricle, PA = pulmonary artery. (Reprinted with permission from Ref. 75).

Future developments will include the use of higher magnetic field strengths, contrast agents for plaque characterizations (91,92), and studies of vessel wall thickness following interventions (93).

### **High-Field Coronary Imaging**

In MRI the SNR is theoretically proportional to the field strength of the static magnetic field,  $B_0$  (94). Therefore, high-field 3T systems, which have recently been approved by the FDA, will be useful for enhancing SNR for many cardiovascular applications (95). Increased SNR will not only enhance detail visibility, it will also support the acquisition of higher spatial and temporal resolution images, and abbreviate scanning times. At 3T, an approximately twofold increase in SNR is expected compared to 1.5T systems. This can theoretically result in a fourfold reduction (in practice, this reduction factor is limited by the coil geometry, or  $g$ -factor) in scanning time using simultaneous acquisition of spatial harmonics (SMASH) (96) or sensitivity encoding (SENSE) (97). Abbreviated scanning times can be used to shorten breath-hold durations, for more SNR-efficient bolus contrast agent-enhanced imaging (98), increased temporal resolution, or enhanced volumetric coverage. A further advantage of high-field MRI is the prolonged T1 values. This makes the use of spin-labeling techniques

particularly attractive since these techniques not only can take advantage of the enhanced SNR, they can also result in less decay of the labeled information. Undoubtedly, the advantages associated with higher field strength will also open new avenues for research, development, and discoveries for many years to come. Therefore, a number of research centers have already performed cardiovascular MRI at 3T. One of the major problems with 3T includes reliable R-wave triggering. At higher field strength, the magneto-hydrodynamic effect is enhanced and an artifactual voltage overlaid on the T-wave of the ECG results. Since this artifactual augmentation of the T-wave may frequently mislead the R-wave detection algorithm, triggering is performed on the T-wave instead of the R-wave. However, with sophisticated R-wave detection algorithms (99), artifactual T-wave augmentation originating from the magneto-hydrodynamic effect can be identified, and “true” R-wave detection has become very reliable. An initial implementation of coronary MRA in healthy adult subjects and at 3T has been reported (100), and a 90% improvement in spatial resolution was obtained with no loss in SNR compared to earlier multicenter trial patient data (48). Specifically, the approximately twofold improvement in SNR not only can result in enhanced spatial resolution, it can also, with the use of parallel

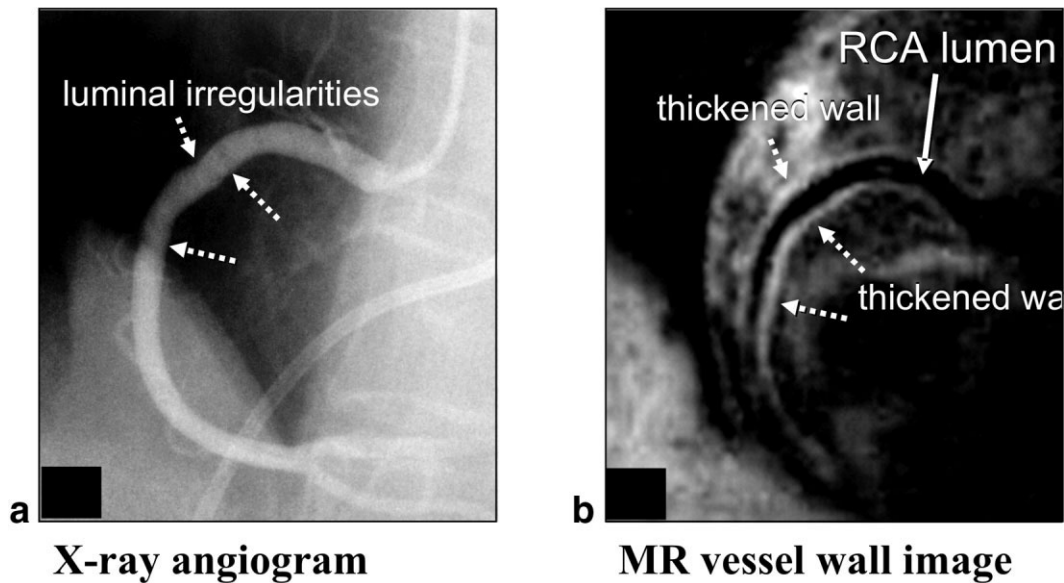


**Figure 14.** X-ray angiogram (a) and spiral MR coronary vessel wall image obtained with a local dual-inversion technique (b) in a patient with (X-ray angiographically) nonsignificant CAD. The RCA is visualized and a long contiguous segment of the coronary artery vessel wall appears signal-enhanced while the lumen blood pool is signal-suppressed because of the local dual-inversion prepulse. In the area of the luminal irregularities observed on the X-ray (a, dashed arrows), focal thickening of the vessel wall is observed on the MR vessel wall image (b, dashed arrows). *Circulation* 2002 Jul 16;106:296–9. (Reprinted with permission from Ref. 89).

imaging (SENSE), result in enhanced temporal resolution and reduced scanning times, which are most important factors in further minimizing residual myocardial motion artifacts (101). However, while the feasibility of coronary MRA at 3T has been demonstrated with (102) and without (100) the use of endogenous contrast enhancement (Fig. 15), the limits of spatial resolution are neither defined nor explored, and the benefits of prolonged T1 values remain to be evaluated for coronary imaging. In a preliminary study in which the diagnostic value of 3T for identifying CAD was investigated in direct comparison with 1.5T, no significant improvements at the higher magnetic field strength were reported (103). However, the use of more sophisticated shimming algorithms (104) and adiabatic T2 preparation (105) will likely contribute to further improved results at high magnetic field strength.

As the first 7T systems ready for human use begin to be installed, B0- and B1-related artifacts will increase, and reliable ECG triggering will become even more challenging (99).

### Surface Coil Arrays

In most patient and volunteer studies, surface coils with a limited number of coil elements have been used for coronary MRA. With simultaneous progress in the areas of receiver architecture and large coil arrays, we can expect higher acceleration factors and improvements in SNR by exploiting this technology. It has already been demonstrated that experimental coil designs with up to 32 elements lead to SNR improvements that enable whole-heart coverage with a relatively high spatial resolution in a single breath-hold (106). However, such coil arrays are currently not widely available,

and they remain to be optimized for cardiac applications. Furthermore, cabling and data handling are challenging engineering tasks that need to be addressed to improve usability. However, the preliminary data obtained with experimental 16- or 32-channel architecture have triggered interest in the field, and this technology will most likely contribute to further improvements in coronary MRA.

### Metallic Artifacts

The more widespread use of coated and drug-eluting intracoronary stents poses a challenge to MRI. While it is considered safe to image patients after stent placement, stents are often made from stainless steel, which generates a local magnetic field susceptibility that generally appears as an area of artifactual signal voids on MR images. These artifacts depend on the material of the stent (108) and on the imaging sequence that is being used. Typically, the image artifacts extend beyond the stents on gradient-echo imaging sequences, while this area of signal void can be minimized using FSE imaging techniques (30). However, the development of stents that do not affect image integrity is currently an active field of research (108,109). Similarly to stents, sternal wires and clips are also sources of image artifacts that may adversely affect coronary MRI in general.

### EBCT AND MDCT

The use of EBCT and MDCT to noninvasively image coronary anatomy was recently reviewed in detail (110–113). EBCT has been used for over two decades to detect and quantify coronary artery calcification. Coro-

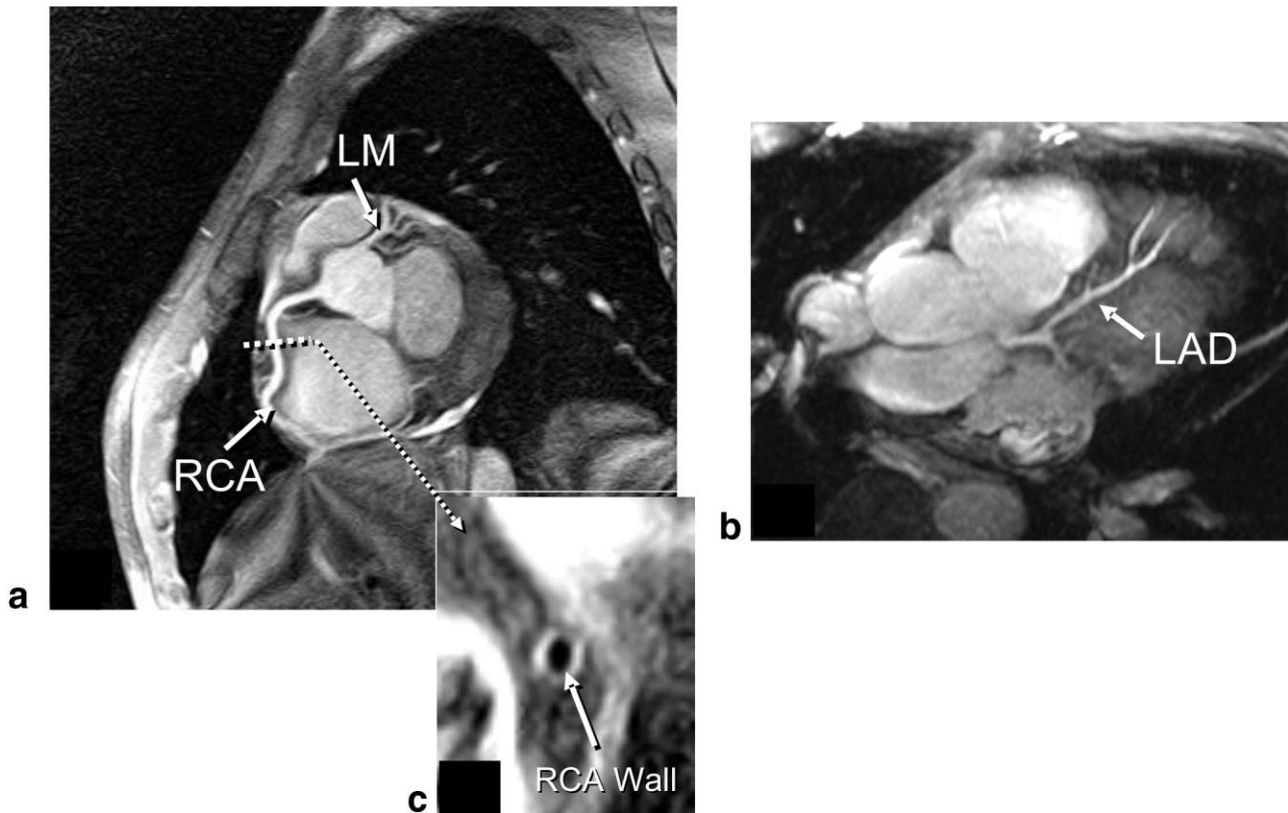


**Figure 15.** High-field coronary images obtained in healthy adult subjects on a 3T system. **a:** RCA system together with the LM and some branching vessels. High visual signal intensity is observed on the RCA. **b:** Coronary vessel wall image acquired perpendicular to the RCA. The lumen blood pool is hypointense, while the circular vessel wall appears hyperintense. Images a and b were obtained during free-breathing using real-time navigator technology. **c:** The left coronary system and LAD display with high signal intensity. The data from image c were obtained during a short period of sustained respiration. (Image c courtesy of D. Li, Northwestern University, and G. Laub, Siemens Medical Solutions.) LM = left main; RCA = right coronary artery; LAD = left anterior descending.

nary calcification is pathognomonic for atherosclerosis and is associated with an increased risk of future cardiac events (110–111). Coronary calcium detection has been proposed for expanded cardiovascular risk stratification in asymptomatic populations, with particular utility for patients with moderate cardiovascular risk (110,114). In patients with chest pain, calcium scores can predict the presence of a significant stenosis and future cardiac events, although the calcium may not localize the culprit lesion (115). Coronary calcium scoring can also be performed with MDCT. However, calcium scoring with EBCT has been more extensively studied, and its reproducibility and lower ionizing radiation exposure have been documented (110).

Unlike coronary MRA, coronary CT angiography (CTA) requires the administration of a contrast agent, which carries a small risk of allergic reaction and impairment of renal function. EBCT offers a temporal resolution approaching 100 msec/slice with a spatial resolution of  $0.35 \times 0.35 \times 1.5$  mm (110). EBCT acquisitions are typically ECG-gated to the portion of the cardiac cycle with the least motion, to limit motion artifacts and exposure to ionizing radiation. MDCT is often performed with retrospective ECG gating, whereby many images are collected but only those from periods of minimal cardiac motion are retained. Heart

rates below 70 per minute improve coronary image quality in MDCT, with a reported temporal resolution of 180–300 msec (110).

A head-to-head comparison of 3D navigator-gated MRI with 16-slice MDCT was recently performed in 52 patients who also underwent invasive quantitative coronary angiography (116). Five of 452 segments could not be analyzed by MRI, and five other segments could not be interpreted by MDCT. By visual assessment, the sensitivity and specificity were high and similar for both technologies on a per-segment and per-vessel basis to detect a >50% stenosis. On a per-patient basis, the findings for sensitivity (92% vs. 88%), specificity (67% vs. 50%), positive predictive value (84% vs. 77%), and negative predictive value (86% vs. 69%) were reported to be similar for both MDCT and MRI, respectively. The main reasons cited for false positives were poor opacification of small vessels and low CNR with MRI, and heavy calcification with MDCT. In a subgroup of segments with heavy calcification ( $N = 82$ ), the sensitivity was 100% but the specificity was 31% for MDCT. Quantitative assessment improved specificity for MDCT but not MRI. The authors concluded that MDCT offers better visualization of the coronary arteries than MRI (116).

Increased numbers of detectors offer improved image quality, and three studies comparing 64-slice MDCT with invasive quantitative coronary angiography have appeared most recently (117–119). Each study evaluated 59–70 patients. Beta-blockers were administered to reduce the heart rate in two studies (118,119), and voxel sizes approaching 0.4 mm were reported. The sensitivity for detecting a >50% stenosis varied between 73% and 95% (117–119). In one study the sensitivity, specificity, and positive and negative predictive values for detecting significant stenoses on a per-patient basis were 95%, 90%, 93%, and 93% (119). Although it is difficult to directly compare these most recent findings with earlier results from four- and 16-slice scanners, it is generally concluded that the diagnostic accuracy is improved with 64-slice MDCT.

The ionizing radiation dose is considerable in such studies and merits mention. In the most recent comparative studies with 64-slice MDCT coronary angiography, the reported mean radiation dose varied between 10–14 mSv (118) and 13–18 mSv (119). For comparison, the effective radiation doses for common radiologic examinations are 0.1 mSv for chest radiography and 3–5 mSv for selective coronary angiography (120). The average annual background radiation in the United States is 3.6 mSv (120). Given that the radiation dose is considerably higher with 64-slice MDCT angiography than with conventional selective coronary angiography, the risks of radiation exposure must be weighed against the potential benefits of this emerging technique, especially in young and middle-aged populations.

## SUMMARY

In coronary MRA, much progress in the suppression of intrinsic and extrinsic myocardial motion has been made, and a variety of effective methods for contrast generation have been reported. While anomalous coronary arteries, aneurysms, and bypass graft patency can be reliably assessed using MRI, it also appears to be of clinical value for assessing native CAD in patients with suspected LM or multivessel disease. In patients referred to selective X-ray coronary angiography, a negative coronary MRA strongly suggests the absence of severe multivessel disease. Even though these results are very encouraging and stimulate further technical and methodological progress, the currently available data do not support the widespread clinical use of contemporary coronary MRA to identify focal coronary stenoses in patients with chest pain at this time. Similarly, coronary MRA may also not yet be adequate for screening of asymptomatic high-risk patients. A further increase in both spatial resolution and CNR may be needed. In this regard, higher magnetic field strengths, contrast agents, and advanced imaging techniques will likely play a major role. However, before an improvement in spatial resolution can benefit the diagnostic value of MRI as a noninvasive tool for the quantitative assessment of native CAD, further progress in the areas of motion suppression and ease-of-use is required.

As compared to coronary MRA, state-of-the-art coronary CTA affords the advantage of a higher spatial res-

olution and improved ease-of-use, since whole-heart coverage is obtained in a single breath-hold. However, exclusive visualization of the vessel wall and coronary flow measurements currently cannot be obtained using CTA. Similarly to breath-hold MRI, CTA image quality depends on the quality of the breath-hold, while diaphragmatic drift and inconsistent end-expiratory position in serial breath-holds are limiting factors. Furthermore, the data-collection period per RR interval should be short for both CTA and MRI, and both modalities benefit equally from regular and low heart rates. While  $\beta$ -blockers are routinely used in CTA, this is currently not routine in MRI and should be considered for patient studies in which CTA and MRA are directly compared. On CT images postcontrast, calcifications are often indistinguishable from the contrast agent in the blood pool, and lesions in the areas of calcifications may not easily be evaluated. Especially in an older population, which is more likely to have coronary calcifications, this may limit the diagnostic value of CTA. While coronary CTA data from single-center studies and selected patient populations look very encouraging, no multicenter data exist at the present time. Finally, in CTA the high doses of radiation and nephrotoxic contrast agent required are a disadvantage, especially for younger patients and follow-up examinations.

## REFERENCES

- Rosamond W, Flegal K, Friday G, et al. Heart disease and stroke statistics—2007 update: a report from the American Heart Association Statistics Committee and Stroke Statistics Subcommittee. *Circulation* 2007;115(5):e69–171.
- Lieberman JM, Botti RE, Nelson AD. Magnetic resonance imaging of the heart. *Radiol Clin North Am* 1984;22:847–858.
- Paulin S, von Schulthess GK, Fossel E, Krayenbuehl HP. MR imaging of the aortic root and proximal coronary arteries. *AJR Am J Roentgenol* 1987;148(4):665–670.
- Edelman RR, Manning WJ, Burstein D, Paulin S. Coronary arteries: breath-hold MR angiography. *Radiology* 1991;181(3):641–643.
- Kim WY, Stuber M, Kissinger KV, Andersen NT, Manning WJ, Botnar RM. Impact of bulk cardiac motion on right coronary MR angiography and vessel wall imaging. *J Magn Reson Imaging* 2001;14(4):383–390.
- Wang Y, Grimm RC, Felmlee JP, Riederer SJ, Ehman RL. Algorithms for extracting motion information from navigator echoes. *Magn Reson Med* 1996;36(1):117–123.
- Jahnke C, Paetsch I, Nehrke K, et al. A new approach for rapid assessment of the cardiac rest period for coronary MRA. *J Cardiovasc Magn Reson* 2005;7(2):395–399.
- Hofman MB, Wickline SA, Lorenz CH. Quantification of in-plane motion of the coronary arteries during the cardiac cycle: implications for acquisition window duration for MR flow quantification. *J Magn Reson Imaging* 1998;8(3):568–576.
- Duerinckx A, Atkinson DP. Coronary MR angiography during peak-systole: work in progress. *J Magn Reson Imaging* 1997;7(6):979–986.
- Wang Y, Grimm RC, Rossman PJ, Debbins JP, Riederer SJ, Ehman RL. 3D coronary MR angiography in multiple breath-holds using a respiratory feedback monitor. *Magn Reson Med* 1995;34(1):11–16.
- Bornert P, Jensen D. Coronary artery imaging at 0.5 T using segmented 3D echo planar imaging. *Magn Reson Med* 1995;34(6):779–785.
- Wielopolski PA, van Geuns RJ, de Feyter PJ, Oudkerk M. Breath-hold coronary MR angiography with volume targeted imaging. *Radiology* 1998;209(1):209–219.
- Goldfarb JW, Edelman RR. Coronary arteries: breath-hold, gadolinium-enhanced, three-dimensional MR angiography. *Radiology* 1998;206(3):830–834.

14. van Geuns RJ, Wielopolski PA, de Bruin HG, et al. MR coronary angiography with breath-hold targeted volumes: preliminary clinical results. *Radiology* 2000;217(1):270–277.
15. Stuber M, Botnar RM, Danias PG, Kissinger KV, Manning WJ. Breathhold three-dimensional coronary magnetic resonance angiography using real-time navigator technology. *J Cardiovasc Magn Reson* 1999;1(3):233–238.
16. Danias PG, Stuber M, Botnar RM, Kissinger KV, Chuang ML, Manning WJ. Navigator assessment of breath-hold duration: impact of supplemental oxygen and hyperventilation. *AJR Am J Roentgenol* 1998;171(2):395–397.
17. Liu YL, Riederer SJ, Rossman PJ, Grimm RC, Debbins JP, Ehman RL. A monitoring, feedback, and triggering system for reproducible breath-hold MR imaging. *Magn Reson Med* 1993;30(4):507–511.
18. Ehman RL, Felmlee JP. Adaptive technique for high-definition MR imaging of moving structures. *Radiology* 1989;173(1):255–263.
19. Li D, Kaushikkar S, Haacke EM, et al. Coronary arteries: three-dimensional MR imaging with retrospective respiratory gating. *Radiology* 1996;201(3):857–863.
20. Oshinski JN, Hofland L, Mukundan S Jr, Dixon WT, Parks WJ, Pettigrew RI. Two-dimensional coronary MR angiography without breath holding. *Radiology* 1996;201(3):737–743.
21. McConnell MV, Khasgiwala VC, Savord BJ, et al. Prospective adaptive navigator correction for breath-hold MR coronary angiography. *Magn Reson Med* 1997;37(1):148–152.
22. Stuber M, Botnar RM, Danias PG, Kissinger KV, Manning WJ. Submillimeter three-dimensional coronary MR angiography with real-time navigator correction: comparison of navigator locations. *Radiology* 1999;212(2):579–587.
23. Deshpande VS, Shea SM, Laub G, Simonetti OP, Finn JP, Li D. 3D magnetization-prepared true-FISP: a new technique for imaging coronary arteries. *Magn Reson Med* 2001;46(3):494–502.
24. Jahnke C, Paetsch I, Nehrke K, et al. Rapid and complete coronary arterial tree visualization with magnetic resonance imaging: feasibility and diagnostic performance. *Eur Heart J* 2005.
25. Edelman RR, Chien D, Kim D. Fast selective black blood MR imaging. *Radiology* 1991;181(3):655–660.
26. Brittain JH, Hu BS, Wright GA, Meyer CH, Macovski A, Nishimura DG. Coronary angiography with magnetization-prepared T2 contrast. *Magn Reson Med* 1995;33(5):689–696.
27. Li D, Dolan RP, Walovitch RC, Lauffer RB. Three-dimensional MRI of coronary arteries using an intravascular contrast agent. *Magn Reson Med* 1998;39:1014–1018.
28. Li D, Paschal CB, Haacke EM, Adler LP. Coronary arteries: three-dimensional MR imaging with fat saturation and magnetization transfer contrast. *Radiology* 1993;187(2):401–406.
29. Botnar RM, Stuber M, Danias PG, Kissinger KV, Manning WJ. Improved coronary artery definition with T2-weighted, free-breathing, three-dimensional coronary MRA. *Circulation* 1999;99(24):3139–3148.
30. Stuber M, Botnar RM, Kissinger KV, Manning WJ. Free-breathing black-blood coronary MR angiography: initial results. *Radiology* 2001;219(1):278–283.
31. Stuber M, Botnar RM, Spuentrup E, Kissinger KV, Manning WJ. Three-dimensional high-resolution fast spin-echo coronary magnetic resonance angiography. *Magn Reson Med* 2001;45(2):206–211.
32. Hofman MBM, Henson RE, Kovacs SJ, et al. Blood pool agent strongly improves 3D magnetic resonance coronary angiography using an inversion pre-pulse. *Magn Reson Med* 1999;41(2):360–367.
33. Stuber M, Botnar RM, Danias PG, et al. Contrast agent-enhanced, free-breathing, three-dimensional coronary magnetic resonance angiography. *J Magn Reson Imaging* 1999;10(5):790–799.
34. Huber ME, Paetsch I, Schnackenburg B, et al. Performance of a new gadolinium-based intravascular contrast agent in free-breathing inversion-recovery 3D coronary MRA. *Magn Reson Med* 2003;49(1):115–121.
35. Meyer CH, Hu BS, Nishimura DG, Macovski A. Fast spiral coronary artery imaging. *Magn Reson Med* 1992;28(2):202–213.
36. Bornert P, Stuber M, Botnar RM, et al. Direct comparison of 3D spiral vs. Cartesian gradient-echo coronary magnetic resonance angiography. *Magn Reson Med* 2001;46(4):789–794.
37. Maintz D, Aepfelbacher FC, Kissinger KV, et al. Coronary MR angiography: comparison of quantitative and qualitative data from four techniques. *AJR Am J Roentgenol* 2004;182(2):515–521.
38. Maintz D, Botnar RM, Manning WJ, Stuber M. Images in cardiovascular medicine. Pitfalls in coronary magnetic resonance angiography: right coronary artery occlusion. *Circulation* 2005;111(5):e94–96.
39. Deshpande VS, Li D. Contrast-enhanced coronary artery imaging using 3D trueFISP. *Magn Reson Med* 2003;50(3):570–577.
40. Spuentrup E, Bornert P, Botnar RM, Groen JP, Manning WJ, Stuber M. Navigator-gated free-breathing three-dimensional balanced fast field echo (TrueFISP) coronary magnetic resonance angiography. *Invest Radiol* 2002;37(11):637–642.
41. Weber OM, Martin AJ, Higgins CB. Whole-heart steady-state free precession coronary artery magnetic resonance angiography. *Magn Reson Med* 2003;50(6):1223–1228.
42. Spuentrup E, Katoh M, Buecker A, et al. Free-breathing 3D steady-state free precession coronary MR angiography with radial k-space sampling: comparison with cartesian k-space sampling and cartesian gradient-echo coronary MR angiography—pilot study. *Radiology* 2004;231(2):581–586.
43. Spuentrup E, Katoh M, Stuber M, et al. Coronary MR imaging using free-breathing 3D steady-state free precession with radial k-space sampling. *Rofo* 2003;175(10):1330–1334.
44. Stehning C, Bornert P, Nehrke K, Eggers H, Dossel O. Fast isotropic volumetric coronary MR angiography using free-breathing 3D radial balanced FFE acquisition. *Magn Reson Med* 2004;52(1):197–203.
45. Bi X, Deshpande V, Simonetti O, Laub G, Li D. Three-dimensional breathhold SSFP coronary MRA: a comparison between 1.5T and 3.0T. *J Magn Reson Imaging* 2005;22(2):206–212.
46. Kaul MG, Stork A, Bansmann PM, et al. Evaluation of balanced steady-state free precession (TrueFISP) and k-space segmented gradient echo sequences for 3D coronary MR angiography with navigator gating at 3 Tesla. *Rofo* 2004;176(11):1560–1565.
47. Stuber M, Botnar RM, Danias PG, et al. Double-oblique free-breathing high resolution three-dimensional coronary magnetic resonance angiography. *J Am Coll Cardiol* 1999;34(2):524–531.
48. Kim WY, Danias PG, Stuber M, et al. Coronary magnetic resonance angiography for the detection of coronary stenoses. *N Engl J Med* 2001;345(26):1863–1869.
49. Sakuma H, Ichikawa Y, Suzawa N, et al. Assessment of coronary arteries with total study time of less than 30 minutes by using whole-heart coronary MR angiography. *Radiology* 2005;237(1):316–321.
50. Jhooti P, Gatehouse PD, Keegan J, Bunce NH, Taylor AM, Firmin DN. Phase ordering with automatic window selection (PAWS): a novel motion-resistant technique for 3D coronary imaging. *Magn Reson Med* 2000;43(3):470–480.
51. Huber ME, Hengesbach D, Botnar RM, et al. Motion artifact reduction and vessel enhancement for free-breathing navigator-gated coronary MRA using 3D k-space reordering. *Magn Reson Med* 2001;45(4):645–652.
52. Nehrke K, Bornert P, Manke D, Bock JC. Free-breathing cardiac MR imaging: study of implications of respiratory motion—initial results. *Radiology* 2001;220(3):810–815.
53. Hackenbroch M, Nehrke K, Gieseke J, et al. 3D motion adapted gating (3D MAG): a new navigator technique for accelerated acquisition of free breathing navigator gated 3D coronary MR-angiography. *Eur Radiol* 2005;15(8):1598–1606.
54. Nehrke K, Bornert P, Mazurkewitz P, Winkelmann R, Grasslin I. Free-breathing whole-heart coronary MR angiography on a clinical scanner in four minutes. *J Magn Reson Imaging* 2006;23(5):752–756.
55. Niendorf T, Hardy CJ, Giaquinto RO, et al. Toward single breathhold whole-heart coverage coronary MRA using highly accelerated parallel imaging with a 32-channel MR system. *Magn Reson Med* 2006;56(1):167–176.
56. Buehrer M, Huber ME, Wiesinger F, Boesiger P, Kozerke S. Coil setup optimization for 2D-SENSE whole-heart coronary imaging. *Magn Reson Med* 2006;55(2):460–464.
57. Etienne A, Botnar RM, Van Muiswinkel AM, Boesiger P, Manning WJ, Stuber M. “Soap-Bubble” visualization and quantitative analysis of 3D coronary magnetic resonance angiograms. *Magn Reson Med* 2002;48(4):658–666.
58. Stuber M, Bornert P, Spuentrup E, Botnar RM, Manning WJ. Selective three-dimensional visualization of the coronary arterial lumen using arterial spin tagging. *Magn Reson Med* 2002;47(2):322–329.

59. Danias PG, Stuber M, Edelman RR, Manning WJ. Coronary MRA: a clinical experience in the United States. *J Magn Reson Imaging* 1999;10(5):713-720.
60. Manning WJ, Edelman RR. Magnetic resonance coronary angiography. *Magn Reson Q* 1993;9(3):131-151.
61. Scheidegger MB, Muller R, Boesiger P. Magnetic resonance angiography: methods and its applications to the coronary arteries. *Technol Health Care* 1994;2(4):255-265.
62. McConnell MV, Ganz P, Selwyn AP, Li W, Edelman RR, Manning WJ. Identification of anomalous coronary arteries and their anatomic course by magnetic resonance coronary angiography. *Circulation* 1995;92(11):3158-3162.
63. McConnell MV, Stuber M, Manning WJ. Clinical role of coronary magnetic resonance angiography in the diagnosis of anomalous coronary arteries. *JCMR* 2000;2(3):217-224.
64. Greil GF, Stuber M, Botnar RM, et al. Coronary magnetic resonance angiography in adolescents and young adults with Kawasaki disease. *Circulation* 2002;105(8):908-911.
65. Manning WJ, Li W, Edelman RR. A preliminary report comparing magnetic resonance coronary angiography with conventional angiography. *N Engl J Med* 1993;328(12):828-832.
66. Duerinckx AJ, Urman MK. Two-dimensional coronary MR angiography: analysis of initial clinical results. *Radiology* 1994;193(3):731-738.
67. Post JC, van Rossum AC, Hofman MB, Valk J, Visser CA. Three-dimensional respiratory-gated MR angiography of coronary arteries: comparison with conventional coronary angiography. *AJR Am J Roentgenol* 1996;166(6):1399-1404.
68. Müller MF, Fleisch M, Kroeker R, Chatterjee T, Meier B, Vock P. Proximal coronary artery stenosis: three-dimensional MRI with fat saturation and navigator echo. *J Magn Reson Imaging* 1997;7(4):644-651.
69. Post JC, van Rossum AC, Hofman MB, de Cock CC, Valk J, Visser CA. Clinical utility of two-dimensional magnetic resonance angiography in detecting coronary artery disease. *Eur Heart J* 1997;18(3):426-433.
70. Pennell DJ, Bogren HG, Keegan J, Firmin DN, Underwood SR. Assessment of coronary artery stenosis by magnetic resonance imaging. *Heart* 1996;75(2):127-133.
71. White RD, Caputo GR, Mark AS, Modin GW, Higgins CB. Coronary artery bypass graft patency: noninvasive evaluation with MR imaging. *Radiology* 1987;164(3):681-686.
72. Aurigemma GP, Reichel N, Axel L, Schiebler M, Harris C, Kressel HY. Noninvasive determination of coronary artery bypass graft patency by cine magnetic resonance imaging. *Circulation* 1989;80(6):1595-1602.
73. von Smekal A, Knez A, Seelos KC, et al. [A comparison of ultrafast computed tomography, magnetic resonance angiography and selective angiography for the detection of coronary bypass patency]. *Rofo Fortschr Geb Rontgenstr Neuen Bildgeb Verfahr* 1997;166(3):185-191.
74. Kessler W, Achenbach S, Moshage W, et al. Usefulness of respiratory gated magnetic resonance coronary angiography in assessing narrowings  $>$  or  $=$  50% in diameter in native coronary arteries and in aortocoronary bypass conduits. *Am J Cardiol* 1997;80(8):989-993.
75. Langerak SE, Vliegen HW, de Roos A, et al. Detection of vein graft disease using high-resolution magnetic resonance angiography. *Circulation* 2002;105(3):328-333.
76. Clarke GD, Eckels R, Chaney C, et al. Measurement of absolute epicardial coronary artery flow and flow reserve with breath-hold cine phase-contrast magnetic resonance imaging. *Circulation* 1995;91(10):2627-2634.
77. Clarke GD, Hundley WG, McColl RW, et al. Velocity-encoded, phase-difference cine MRI measurements of coronary artery flow: dependence of flow accuracy on the number of cine frames. *J Magn Reson Imaging* 1996;6(5):733-742.
78. Hofman MB, van Rossum AC, Sprenger M, Westerhof N. Assessment of flow in the right human coronary artery by magnetic resonance phase contrast velocity measurement: effects of cardiac and respiratory motion. *Magn Reson Med* 1996;35(4):521-531.
79. Wedding KL, Grist TM, Foltz JD, et al. Coronary flow and flow reserve in canines using MR phase difference and complex difference processing. *Magn Reson Med* 1998;40(5):656-665.
80. Hundley WG, Lange RA, Clarke GD, et al. Assessment of coronary arterial flow and flow reserve in humans with magnetic resonance imaging. *Circulation* 1996;93(8):1502-1508.
81. Hundley WG, Hamilton CA, Clarke GD, et al. Visualization and functional assessment of proximal and middle left anterior descending coronary stenoses in humans with magnetic resonance imaging. *Circulation* 1999;99(25):3248-3254.
82. Nagel E, Bornstedt A, Hug J, Schnackenburg B, Wellenhofer E, Fleck E. Noninvasive determination of coronary blood flow velocity with magnetic resonance imaging: comparison of breath-hold and navigator techniques with intravascular ultrasound. *Magn Reson Med* 1999;41(3):544-549.
83. Shibata M, Sakuma H, Isaka N, Takeda K, Higgins CB, Nakano T. Assessment of coronary flow reserve with fast cine phase contrast magnetic resonance imaging: comparison with measurement by Doppler guide wire. *J Magn Reson Imaging* 1999;10(4):563-568.
84. Bedaux WL, Hofman MB, de Cock CC, Stoel MG, Visser CA, van Rossum AC. Magnetic resonance imaging versus Doppler guide wire in the assessment of coronary flow reserve in patients with coronary artery disease. *Coron Artery Dis* 2002;13(7):365-372.
85. Nagel E, Thouet T, Klein C, et al. Noninvasive determination of coronary blood flow velocity with cardiovascular magnetic resonance in patients after stent deployment. *Circulation* 2003;107(13):1738-1743.
86. Fayad ZA, Fuster V, Fallon JT, et al. Noninvasive in vivo human coronary artery lumen and wall imaging using black-blood magnetic resonance imaging. *Circulation* 2000;102(5):506-510.
87. Botnar RM, Stuber M, Kissinger KV, Kim WY, Spuentrup E, Manning WJ. Noninvasive coronary vessel wall and plaque imaging with magnetic resonance imaging. *Circulation* 2000;102(21):2582-2587.
88. Botnar RM, Kim WY, Bornert P, Stuber M, Spuentrup E, Manning WJ. 3D coronary vessel wall imaging utilizing a local inversion technique with spiral image acquisition. *Magn Reson Med* 2001;46(5):848-854.
89. Kim WY, Stuber M, Bornert P, Kissinger KV, Manning WJ, Botnar RM. Three-dimensional black-blood cardiac magnetic resonance coronary vessel wall imaging detects positive arterial remodeling in patients with nonsignificant coronary artery disease. *Circulation* 2002;106(3):296-299.
90. Glagov S, Weisenberg E, Zarins CK, Stankunavicius R, Kolettis GJ. Compensatory enlargement of human atherosclerotic coronary arteries. *N Engl J Med* 1987;316(22):1371-1375.
91. Yuan C, Kerwin WS, Ferguson MS, et al. Contrast-enhanced high resolution MRI for atherosclerotic carotid artery tissue characterization. *J Magn Reson Imaging* 2002;15(1):62-67.
92. Wasserman BA, Smith WI, Trout 3rd HH, Cannon 3rd RO, Balaban RS, Arai AE. Carotid artery atherosclerosis: in vivo morphologic characterization with gadolinium-enhanced double-oblique MR imaging initial results. *Radiology* 2002;223(2):566-573.
93. Nissen SE, Tsunoda T, Tuzcu EM, et al. Effect of recombinant ApoA-I Milano on coronary atherosclerosis in patients with acute coronary syndromes: a randomized controlled trial. *JAMA* 2003;290(17):2292-2300.
94. Singerman RW, Denison TJ, Wen H, Balaban RS. Simulation of B1 field distribution and intrinsic signal-to-noise in cardiac MRI as a function of static magnetic field. *J Magn Reson* 1997;125(1):72-83.
95. Dougherty L, Connick TJ, Mizsei G. Cardiac imaging at 4 Tesla. *Magn Reson Med* 2001;45(1):176-178.
96. Sodickson DK, Manning WJ. Simultaneous acquisition of spatial harmonics (SMASH): fast imaging with radiofrequency coil arrays. *Magn Reson Med* 1997;38(4):591-603.
97. Pruessmann KP, Weiger M, Scheidegger MB, Boesiger P. SENSE: sensitivity encoding for fast MRI. *Magn Reson Med* 1999;42(5):952-962.
98. Sodickson DK, McKenzie CA, Li W, Wolff S, Manning WJ, Edelman RR. Contrast-enhanced 3D MR angiography with simultaneous acquisition of spatial harmonics: a pilot study. *Radiology* 2000;217(1):284-289.
99. Fischer SE, Wickline SA, Lorenz CH. Novel real-time R-wave detection algorithm based on the vectorcardiogram for accurate gated magnetic resonance acquisitions. *Magn Reson Med* 1999;42(2):361-370.
100. Stuber M, Botnar RM, Fischer SE, et al. Preliminary report on in vivo coronary MRA at 3 Tesla in humans. *Magn Reson Med* 2002;48(3):425-429.
101. Huber ME, Kozerke S, Pruessmann KP, Smink J, Boesiger P. Sensitivity-encoded coronary MRA at 3T. *Magn Reson Med* 2004;52(2):221-227.

102. Bi X, Li D. Coronary arteries at 3.0 T: contrast-enhanced magnetization-prepared three-dimensional breathhold MR angiography. *J Magn Reson Imaging* 2005;21(2):133-139.
103. Sommer T, Hackenbroch M, Hofer U, et al. Coronary MR angiography at 3.0 T versus that at 1.5 T: initial results in patients suspected of having coronary artery disease. *Radiology* 2005;234(3):718-725.
104. Schar M, Kozerke S, Fischer SE, Boesiger P. Cardiac SSFP imaging at 3 Tesla. *Magn Reson Med* 2004;51(4):799-806.
105. Nezafat R, Ouwerkerk R, Gharib AM, Pettigrew RI, McVeigh ER, Stuber M. B1 insensitive T2Preparation sequence for coronary imaging at 3T. *Proc Intl Soc Mag Reson Med (abstract)* 2005:2794.
106. Niendorf T, Sodickson DK, Hardy CJ, et al. Towards whole heart coverage in a single breath-hold: Coronary artery imaging using a true 32-channel phased array MRI system. 2004; Kyoto, Japan ISMRM. p 703.
107. Maintz D, Botnar RM, Fischbach R, Heindel W, Manning WJ, Stuber M. Coronary magnetic resonance angiography for assessment of the stent lumen: a phantom study. *J Cardiovasc Magn Reson* 2002;4(3):359-367.
108. Spuentrup E, Ruebben A, Mahnken A, et al. Artifact-free coronary magnetic resonance angiography and coronary vessel wall imaging in the presence of a new, metallic, coronary magnetic resonance imaging stent. *Circulation* 2005;111(8):1019-1026.
109. Buecker A, Spuentrup E, Ruebben A, et al. New metallic MR stents for artifact-free coronary MR angiography: feasibility study in a swine model. *Invest Radiol* 2004;39(5):250-253.
110. Budoff MJ. Atherosclerosis imaging and calcified plaque: coronary artery disease risk assessment. *Prog Cardiovasc Dis* 2003;46(2):135-148.
111. Budoff MJ, Cohen MC, Garcia MJ, et al. ACCF/AHA clinical competence statement on cardiac imaging with computed tomography and magnetic resonance: a report of the American College of Cardiology Foundation/American Heart Association/American College of Physicians Task Force on Clinical Competence and Training. *J Am Coll Cardiol* 2005;46(2):383-402.
112. Fayad ZA, Sirol M, Nikolaou K, Choudhury RP, Fuster V. Magnetic resonance imaging and computed tomography in assessment of atherosclerotic plaque. *Curr Atheroscler Rep* 2004;6(3):232-242.
113. Achenbach S, Daniel WG. Imaging of coronary atherosclerosis using computed tomography: current status and future directions. *Curr Atheroscler Rep* 2004;6(3):213-218.
114. Greenland P, LaBree L, Azen SP, Doherty TM, Detrano RC. Coronary artery calcium score combined with Framingham score for risk prediction in asymptomatic individuals. *JAMA* 2004;291(2):210-215.
115. Georgiou D, Budoff MJ, Kaufer E, Kennedy JM, Lu B, Brundage BH. Screening patients with chest pain in the emergency department using electron beam tomography: a follow-up study. *J Am Coll Cardiol* 2001;38(1):105-110.
116. Kefer J, Coche E, Legros G, et al. Head-to-head comparison of three-dimensional navigator-gated magnetic resonance imaging and 16-slice computed tomography to detect coronary artery stenosis in patients. *J Am Coll Cardiol* 2005;46(1):92-100.
117. Leschka S, Alkadhi H, Plass A, et al. Accuracy of MSCT coronary angiography with 64-slice technology: first experience. *Eur Heart J* 2005;26(15):1482-1487.
118. Leber AW, Knez A, von Ziegler F, et al. Quantification of obstructive and nonobstructive coronary lesions by 64-slice computed tomography: a comparative study with quantitative coronary angiography and intravascular ultrasound. *J Am Coll Cardiol* 2005;46(1):147-154.
119. Raff GL, Gallagher MJ, O'Neill WW, Goldstein JA. Diagnostic accuracy of noninvasive coronary angiography using 64-slice spiral computed tomography. *J Am Coll Cardiol* 2005;46(3):552-557.
120. Gerber TC, Kuzo RS, Morin RL. Techniques and parameters for estimating radiation exposure and dose in cardiac computed tomography. *Int J Cardiovasc Imaging* 2005;21(1):165-176.